Experimental investigation of the influence of the FSW plunge processing parameters on the maximum generated force and torque

Sandra Zimmer · Laurent Langlois · Julien Laye · Régis Bigot

Abstract The paper presents the results of an experimental investigation, done on the friction stir welding (FSW) plunging stage. Previous research works showed that the axial force and torque generated during this stage were characteristic for a static qualification of a FSW machine. Therefore, the investigation objectives are to better understand the relation between the processing parameters and the forces and torque generated. One of the goals is to find a way to reduce the maximum axial force and torque occurring at the end of the plunging stage in order to allow the use of a flexible FSW machine. Thus, the influence of the main plunge processing parameters on the maximum axial force and torque are analysed. In fact, forces and torque responses can be influenced by the processing parameter. At the end, a diagram presenting the maximum axial force and torque according to the processing parameters is presented. It is an interesting way to present the experimental results. This kind of representation can be useful for the processing parameters choice. They can be chosen according to the force and torque responses and consequently to the FSW machine capacities.

Keywords Friction stir welding · Plunging stage · FSW machine qualification · Plunging forces and torques

S. Zimmer · L. Langlois (✉) · R. Bigot
Arts et Metiers ParisTech, LCFC,
4 Rue Augustin Fresnel,
57078 Metz, France
e-mail: laurent.langlois@ensam.metz.fr

J. Laye
Institut de Soudure, FSW Center,
2-4 rue Pilâtre de Rozier,
57420 Goin, France

1 Introduction

Friction stir welding (FSW) is an innovative welding process commonly known as a solid state welding process [1]. Its main characteristic is to join material without reaching the fusion temperature. It enables to weld almost all types of aluminium alloys, even the one classified as non-weldable by fusion welding due to hot cracking and poor solidification microstructure in the fusion zone [2]. To perform FSW, a non-consumable rotating tool, composed of a shoulder and a pin, is inserted into the interface of two rigidly clamped workpieces. The tool is moved along the joint once the shoulder is in contact with the workpieces surfaces. The tool rotation and translation generate the material stirring, joining the workpieces together. The required heat energy is provided by the friction between the tool and the workpieces and the severe plastic deformation generated around the tool [2]. Figure 1 presents a schematic drawing of the FSW butt welding.

The main advantages of FSW as compared to fusion welding processes are higher weld mechanical properties, low distortion and its automation and repeatability possibilities [2]. Furthermore, it satisfies the industrials' joining requirements to weld similar or dissimilar aluminium parts together or with other metals like cupper or steel [2]. But, the lack of industrial standards, like the design guidelines, the required welding axial force and the high cost of capital equipment, are barriers to the FSW utilisation [3]. Today, the equipments commonly used to perform FSW are dedicated machines, milling machines or robots. Milling machines and robots are both standard equipments involving a lower investment cost but with limited capacities to perform FSW in terms of forces and stiffness. The welding operation requires high process forces and torque in order to insure the tool kinematics and the material stirring. As

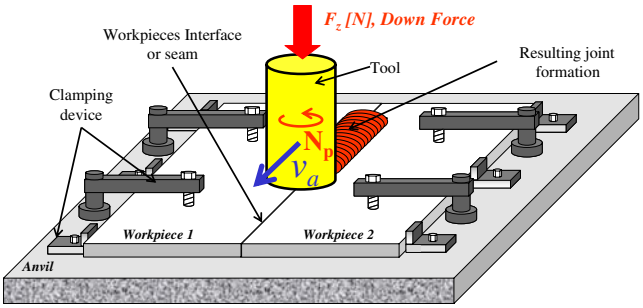

Fig. 1 Schematic drawing of friction stir welding of two plates

the forces and torques are transmitted to the FSW machine, it seems necessary to analyse the tool/workpiece kinematics and the mechanical interactions. By studying globally the welding operation, the plunging stage appeared to be characteristic for a static qualification of a FSW machine [4]. Moreover, in this stage, the tool undergoes more wear effects [5], and it initiates the welding thermo-mechanical conditions [6]. Therefore, it seems important to investigate this stage in order to better understand the relationship between the processing parameters and the resulting mechanical interactions. The objectives are to reduce the forces and torques transmitted to the machine during the plunge in order to enable the use of standard and flexible machine, while ensuring welding productivity.

2 Nomenclature

A tool reference frame, R_O (O, X, Y, Z), was defined such that:

- The vector (O,Z) is collinear with the tool rotational axis.
- The vector (O,X) is perpendicular to (O,Z) and tangent to the joint line.
- The vector (O,Y) is perpendicular to (O,Z) and (O,X) and oriented in order to form an orthogonal reference frame.

Figure 2 presents the tool orthogonal system used in this paper.

The parameters name employed are defined as follows:

N_p	rpm	Spindle rotational speed according to the rotational axis, (O,Z)
v_p	mm/min	Tool plunge velocity in Z direction
a_p	mm/min-s	Plunging acceleration in Z direction
d_p	mm/min-s	Plunging deceleration in Z direction
Δ_z	mm	Plunge depth. Parameterised tool displacement in (O,Z) direction
Δt_p	s	Duration of the plunging stage
F_z	kN	Axial force applied on the tool in the Z direction
F_x	kN	Force perpendicular to F_z and in the direction of (O,X)
F_y	kN	Force perpendicular to F_z and in the direction of (O,Y)
$F_{z\ max}$	kN	Maximum axial force, in the Z direction, obtained during plunging stage
$C_{z\ max}$	Nm	Maximum spindle torque obtained during plunging stage
$E_{dissipated}$	J	Energy dissipated during the plunge stage

3 Description of the plunging stage

The plunging stage corresponds to the beginning of the welding operation. Figure 3 presents a schematic view of stage sequences. At the beginning of the plunge, the tool is placed on the workpiece's top surface and centred on the plates' interface. Both are at room temperature. The two workpieces are rigidly clamped together, near the plunge position, in order to avoid axial and transversal workpiece movements. After being placed into rotation, the tool is moved in the Z axis direction with a velocity v_p (Fig. 3a). Then, the tool begins its immersion inside the cold material. The tool progression generates material significant transformation, due to the high temperatures, stresses [6] and material plastic deformation. This leads to non-negligible tool and workpiece mechanical interactions being characterised by forces and torques applied on the tool. The stage is finished when the parameterised plunging depth, Δ_z, is reached. The tool shoulder is then perfectly in contact with the workpieces' top surface and in the right position to start the welding stage (Fig. 3c). Generally, as the plunge does not provide sufficient heat, it is followed by a dwell time in order to increase the tool and material temperature before welding. Fourment and Guerdoux [7] present, through numerical simulation, the evolution of the temperature fields inside the tool and workpiece during the plunging stage. Their results show that the tool and workpiece temperature increases gradually with the indentation of the pin and then the shoulder inside the workpieces.

4 Plunging and control mode possibilities

Depending on the available FSW machine, the plunge stage can be controlled by:

- Displacement control mode
- Force control mode

The chosen control mode will affect the plunge stage processing parameters, the tool/material mechanical interactions, especially the developed axial force, and the plunge

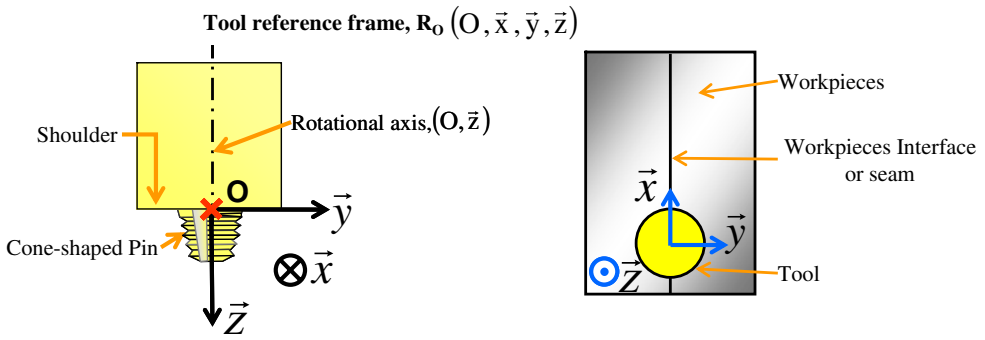

Fig. 2 Specifications of the tool orthogonal frame, R_O (O, X, Y, Z)

duration. The two existing process modes are described below.

4.1 Plunging stage in a force control mode

To perform the plunging stage through a force controlled mode, the used equipment must possess the required controlling mode. For example, a common milling machine cannot perform the operation in this controlling mode. The processing parameters related to this control mode are presented in Fig. 4. When the plunging stage is force controlled, the tool is placed into rotation and a determined force, in the Z direction (F_z), is applied on the tool. The friction between the tool and workpiece generates heat, softening the material. Then, the applied axial force allows the tool to be inserted into the workpieces' interface. In this mode, the major advantage is to control the axial force. Thus, the plunging force can be

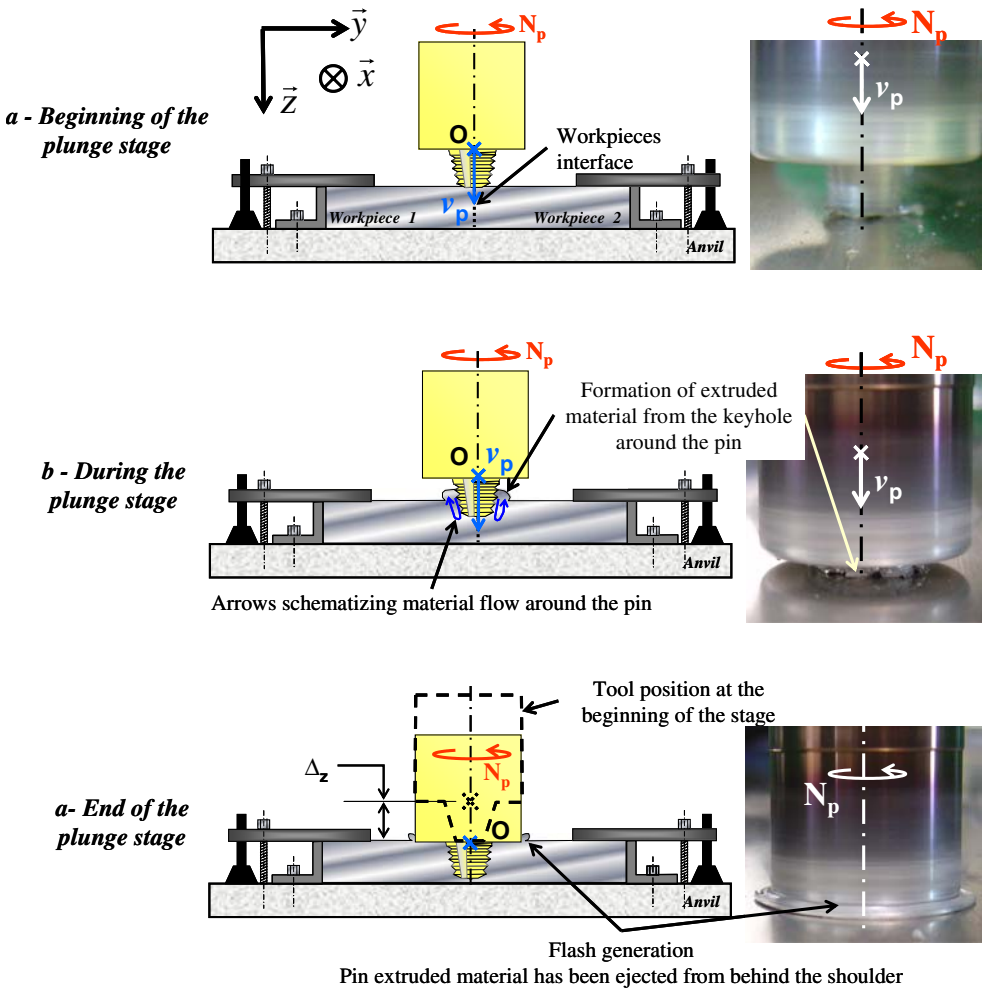

Fig. 3 Illustration of the plunging stage main sequences. **a** Beginning of the plunge stage. **b** During the plunge stage. **c** End of the plunge stage

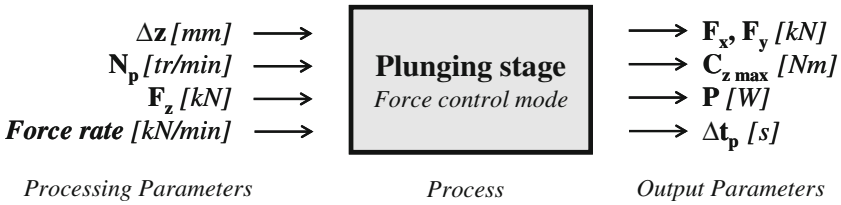

Fig. 4 Processing and output parameters in force controlled plunge mode

chosen according to the welding equipment maximum capacity.

Figure 5 shows a schematic drawing of the processing parameters and the axial in force control plunge mode. It can be seen that the axial force is maintained constant over the whole stage.

In this control mode, the plunge duration Δt_p cannot be directly influenced by one of the processing parameters. Δt_p is a result of the applied processing parameters, the workpiece material responses and the tool geometry.

4.2 Plunging stage in a displacement control mode

The displacement control mode is commonly used for the plunging stage. The processing parameters and the output parameters are given by Fig. 6. Here, the axial force response and its maximum value $F_{z\ max}$ are not directly controlled. However, as showed by Zhang and Zhang [8], the axial pressure applied during the welding stage is an important parameter to achieve a high weld quality. Therefore, the welding axial force and the plunge maximal force obtained at the end of the plunge should have two distinct values. Moreover, Zhang and Zhang's work suggested that it could be interesting to analyse the evolution of the axial pressure during the plunging stage instead of the axial force.

Figure 7a presents a schematic drawing of the processing parameters, and Fig. 7b shows the axial force response. In this mode, the axial movement of the tool is governed by the plunging speed v_p, the acceleration a_p and deceleration d_p. The rotational speed does not influence the tool movement but impacts the tool/workpiece mechanical interactions, i.e. the torque and the forces acting on the tool. Here, the axial force evolution is the workpieces' material response of the applied processing parameters as showed by Santella et al. [9]. So, if the FSW machine has an axial force limit, this limit could be reached. Therefore, it is important to choose processing parameters, leading to acceptable axial force and torque in order to avoid damages of the machine.

The duration of the stage, Δt_p, is directly determined by the plunge velocity value, as presented in Eq. 1.

$$\Delta t_p = \frac{\Delta_z}{v_p} + \frac{v_p}{a_p} = f\left(v_p, a_p, \Delta_z\right) \text{with } d_p = -a_p \quad (1)$$

When the FSW machine can develop the required axial force, to apply the processing parameters, the plunge duration is not influenced by the workpieces' material response. Thus, this mode can be easily used when the process needs to be "time controlled", i.e. when process productivity is searched.

Zimmer et al. [4] identified the maximum axial forces $F_{z\ max}$ and spindle torque $C_{z\ max}$, occurring in the end of this stage, as being characteristic for the static qualification of a FSW machine. Therefore, as the displacement control mode is commonly used in industry, we set up an experimental procedure in order to analyse the influence of the processing parameters on the output parameters (Fig. 6).

5 Calculation of input energy during the plunging stage

As the tool remains at the same position, according to the seam, the heat source remains stationary. Therefore, the area under the spindle power curve represents the mechanical dissipated energy or heat due to friction and material's

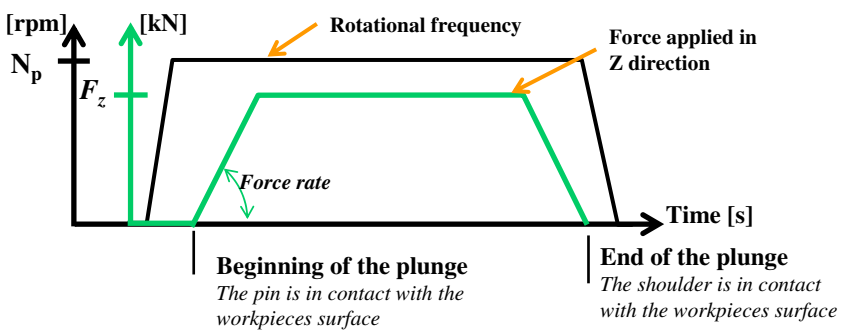

Fig. 5 Schematic drawing of the applied processing parameters in force control mode

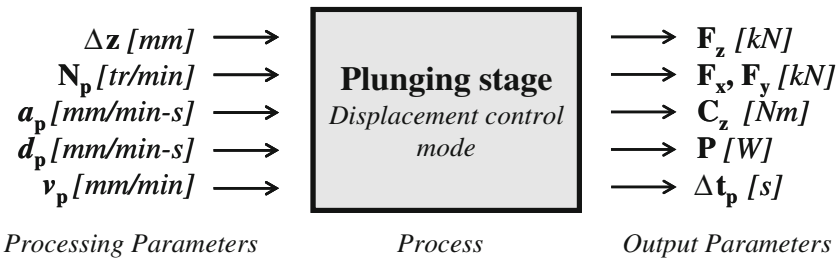

Fig. 6 Processing and output parameters when the plunge is displacement controlled

plastic deformation. This dissipated energy or heat is transmitted to the tool and to the workpiece, increasing their temperature. So, the dissipated heat or energy can be defined as the integral over the time of the spindle mechanical power, since the power related to the tool axial movement is negligible against the total power [4]. The dissipated energy, $E_{\text{dissipated}}$, may be defined by Eq. 2. Thus, at constant plunge velocity v_p, the higher the dissipated energy is, the higher the tool and workpiece temperature will be. The convection and conduction heat dissipation are assumed to be identical from one test to another. So, $E_{\text{dissipated}}$ can be used as a temperature plunge indicator.

$$E_{\text{dissipated}} = \int_{t=0}^{t=\text{end of plunge}} C_z(t) \times \frac{N_p \times 2\pi}{60} dt \quad (2)$$

$$= \text{Area under the power curve}$$

6 Presentation of experimental procedure

The aim of the experimental testing is to evaluate the influence of the parameters N_p and v_p on $F_{z\ max}$ and $C_{z\ max}$, as they are characteristic for a static qualification of a FSW machine.

6.1 Influence of N_p and v_p on $F_{z\ max}$ and $C_{z\ max}$

The starting point, to set up an experimental procedure is the plunging operating point used to perform successful welding operation in a 6-mm-thick 6082-T651 aluminium alloy. This operating point will be called the starting point. So, from this starting point setting of parameters ($N_{p\text{-}0}$, $v_{p\text{-}0}$, $a_{p\text{-}0}$, $d_{p\text{-}0}$, Δ_z), an experimental procedure is built by varying the values of N_p and v_p, firstly by ±33% and secondly by ±66%. The plunge depth Δ_z remains fixed for each tests. Figure 8 presents the applied experimental procedure.

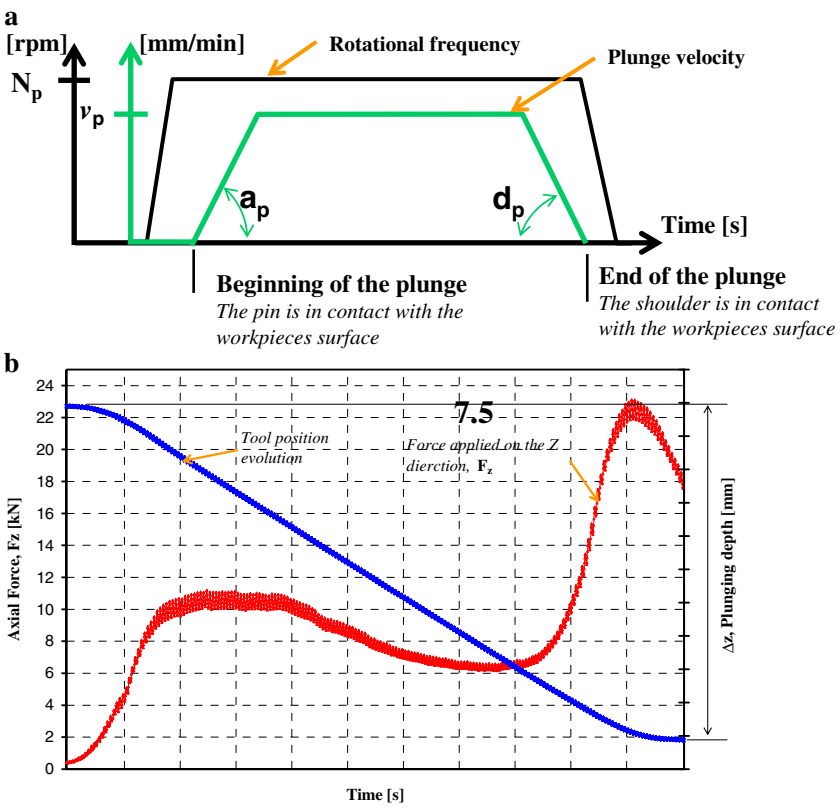

Fig. 7 **a** Schematic drawing of the tool velocities, **b** tool position and axial force response over the time

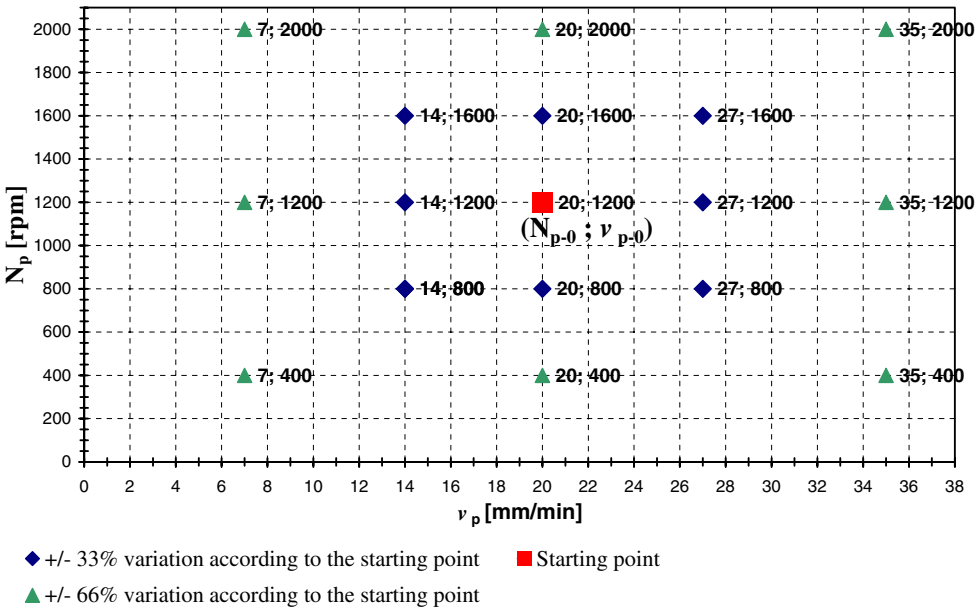

Fig. 8 Presentation of the applied experimental procedure

Tests for each processing parameter were performed three times, and the average value for each point was calculated.

In these experiments, the influence of the tool acceleration or deceleration was not studied. So, in order to avoid the effects of the tool deceleration in the values of $F_{z\ max}$ and $C_{z\ max}$, the acceleration and deceleration has been calibrated in such a way that the acceleration and deceleration distances are equal for each test. Figure 9 presents the schematic drawing of the tool acceleration and deceleration.

At the same time, the axial force and torque responses, according to the processing parameters, are studied through curve analysis.

6.2 Description of the plunge tests

All the tests were performed in one single plate of 6-mm-thick 6082-T651 aluminium alloy series. Figure 10 presents the realisation of plunge testing.

The tool selected was a conventional tool, made of steel, with a concave shoulder and a cone-shaped threaded pin. The tool was tilted by a 2.5° angle. This tool is industrially used to weld 6 mm aluminium alloy. Each test was carried out in the same way and with identical initial thermal conditions. The tool pin was brought in contact with the workpiece's top surface, and a 0.6-kN axial force was applied on it. Then, the tool was put into rotation. Once the tool rotation N_p was reached, the tool was moved with a velocity v_p, in the Z direction. The stage was ended as the tool has been displaced by the value of the plunge depth Δ_z. The tool shoulder is then perfectly in contact with top surface and is in the ideal position to start the welding stage. After 1 s dwell time, the tool was retracted from the plate. The experiments were performed on a MTS-ISTIR-10 Friction Stir Welder, at the Institut de Soudure. This hydraulic machine is fully instrumented, permitting the monitoring of the forces and the spindle torque generated

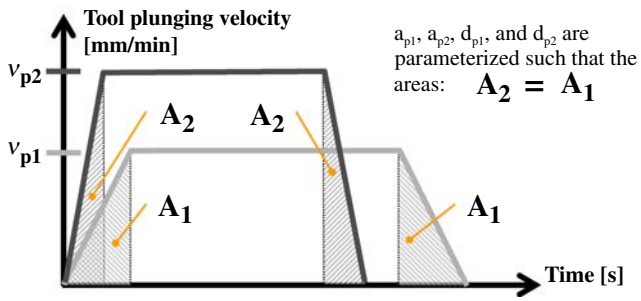

Fig. 9 Schematic drawing of the acceleration and deceleration

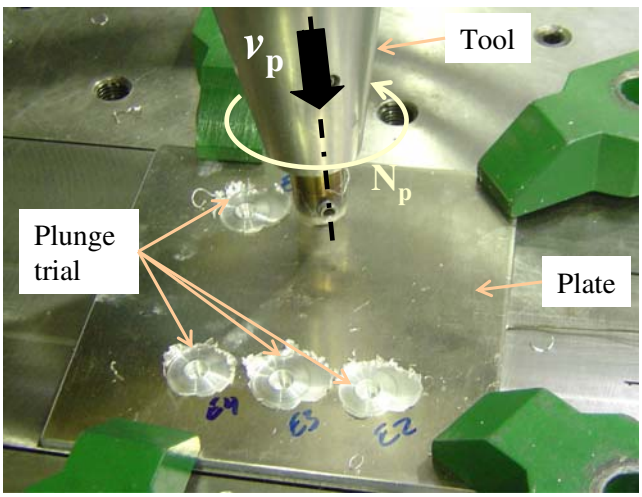

Fig. 10 Presentation of the plunge testing

during FSW process. Figure 11 presents the welding head. The head has several sensors measuring the pressure inside the hydraulic actuators. The values of the forces F_x and F_y, applied on the tool, are calculated from the measured momentum, M_r and M_p. The axial force F_z and the spindle torque C_z are calculated from the actuators placed into the spindle.

The applied experimental procedure explains why the axial force and the spindle torque curve evolutions, presented below, are not equal to zero at the beginning of the plunging stage (Fig. 12).

7 Experimental results and discussions

7.1 Analysis of the forces and spindle torque responses during plunge

Axial force and spindle torque responses are driven by the tool/workpiece mechanical interactions. In the proposed experiment, the influence of the two main parameters, N_p and v_p, will be analysed on the following parameters:

- $F_{z\ max}$ and $C_{z\ max}$, obtained at the end of the plunge
- The general force and torque evolutions according to the plunge depth

Figure 12 shows the axial force and torque applied on the tool during the plunging stage. The analysis of the tool/workpiece interactions is decomposed into three steps. Figure 13 presents pictures of the tool progression and the material flow around the tool, illustrating the plunge progression.

At the beginning of the stage (step 1 on Fig. 12), the axial force rises until it reaches a first peak. It corresponds to the beginning of the pin insertion inside the cold material (Fig. 13a). The peak location and intensity depend on the processing parameters (see Fig. 14). It corresponds to the formation of some ejected debris [10], leading to some material removal (see Fig. 13a). It can be compared to small material removal, occurring during milling. Gerlich et al. [10] explained this material removal by plastic shearing between the tool and the workpieces and the generation and propagation of subsurface cracks leading to the debris formation. Then, the pin progression inside the workpieces generates frictional and material plastic deformation leading to heat generation. This temperature increase softens the material around the pin [10]. Fourment and Guerdoux [7] showed, with plunge numerical simulation, that the workpiece maximum temperature is located at the bottom of the pin. It generates the material softening under the pin [10], facilitating the tool progression. Therefore, it explains the axial force decrease corresponding to step 2 in Fig. 12. Thus, the generated tool/workpiece material mechanical interactions allow the tool to carry on the plunge, without requiring extra axial force. The material softening and the pin immersion generate the upwards displacement of extruded material. It can be seen in Fig. 13b, c. The amount of displaced material should be equivalent to the pin inserted volume [11]. When the tool shoulder comes into contact with the extruded material, the axial forces starts to rise again (step 3 in Fig. 12). The shoulder pushes then the extruded material down to the workpiece surface requiring a significant axial force increase (Fig. 13d, e). The axial force shows a second peak due to the squeezing of the extruded material between the shoulder and the workpiece. Now, the extruded material flows under the shoulder forming a flash around the tool (Fig. 13f). Therefore, this second peak is generally located at the end of the plunging

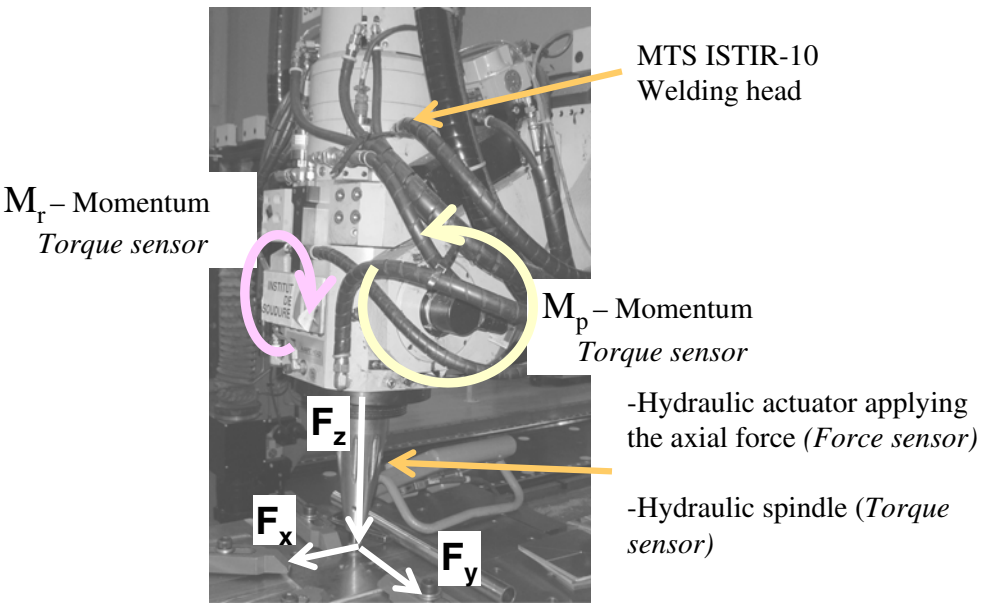

Fig. 11 Welding head and measurement system

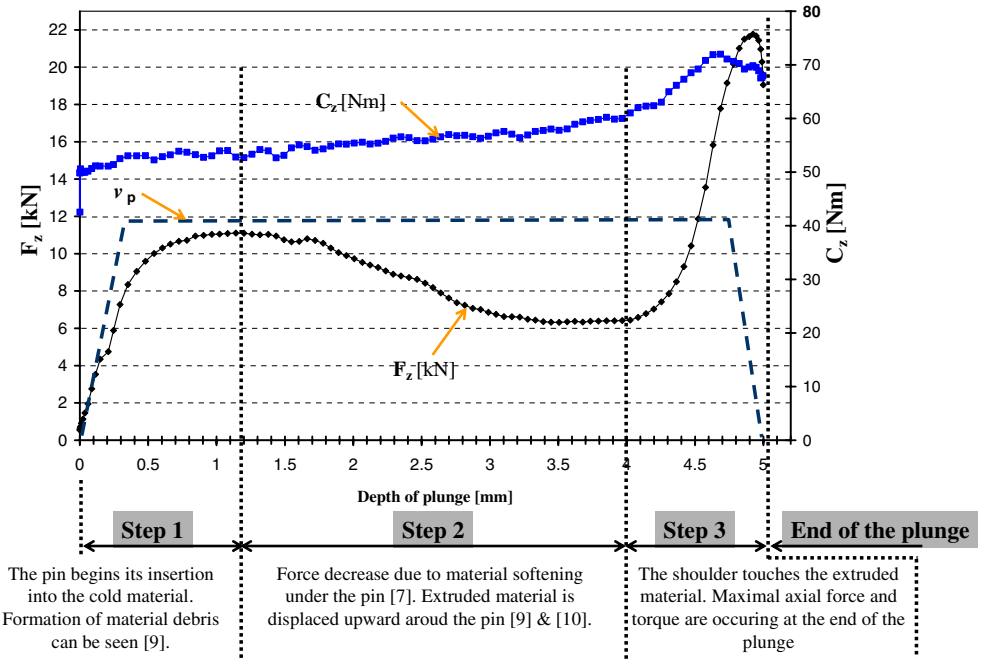

Fig. 12 Evolution of the axial force and the torque according to the plunge depth

stage when the tool shoulder is fully in contact with the workpieces' top surface. The second peak intensity of axial force is generally higher than the first peak. This peak force is characteristic of the plunging stage, and it was already identified in previous research work [10–12].

Compared to the axial force evolution, the spindle torque C_z has a gradual evolution throughout the plunging stage. It can be explained by a gradual pin and workpiece contact area increase leading to an increase of the tool rotational resistance. At the end of the stage, the torque reaches also a peak, when the shoulder touches the workpiece surface. It can be noted that the peak of torque and the second peak of force are appearing quite simultaneously. The curve evolutions are suggesting that no steady state conditions are reached during the stage.

These kinds of axial force and torque evolutions are observed for different processing parameters [5, 10, 12].

7.2 Influence of the processing parameters

Figure 14 presents the force and torque evolution for v_p= 7 mm/min and different rotational frequencies with values, 400, 1,200 and 2,000 rpm. Soundararajan et al. [12] performed some welding experiments on a 6.4-mm- thick 6061-T6 aluminium alloy. His plunge force diagrams have identical general tendencies with the one obtained in our experiment at low rotational frequency, i.e. 400 rpm. The high plunging speed used in his experiment, v_p=133 mm/min, and the shoulder size difference cause the higher recorded axial force values.

However, for N_p=400 rpm, some differences in the axial force and torque evolutions can be noticed (Fig. 14a, b). It is due to the tool/workpiece material mechanical interactions, leading to different temperature and viscosity. Hence, the processing parameters influence the tool/workpiece

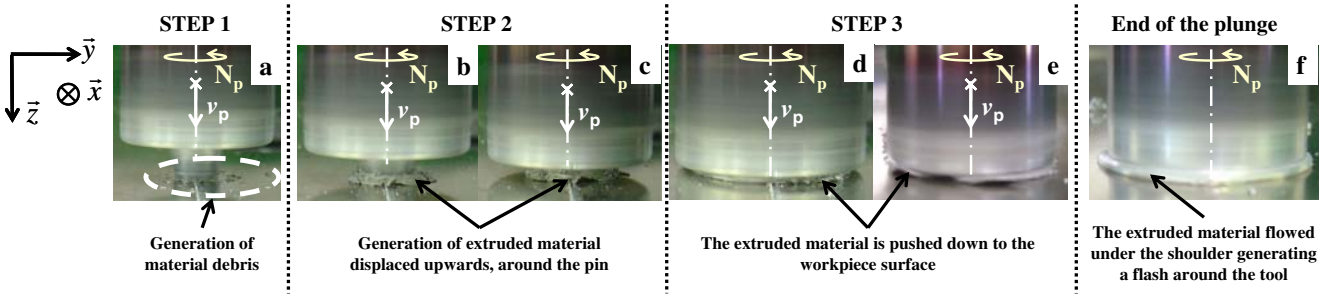

Fig. 13 Visualisation of the tool progression and evolution of the material flow between the workpiece top surface and the tool. **a** Generation of material debris. **b**, **c** Generation of extruded material displaced upwards, around the pin. **d**, **e** The extruded material is pushed down to the workpiece surface. **f** The extruded material flowed under the shoulder, generating a flash around the tool

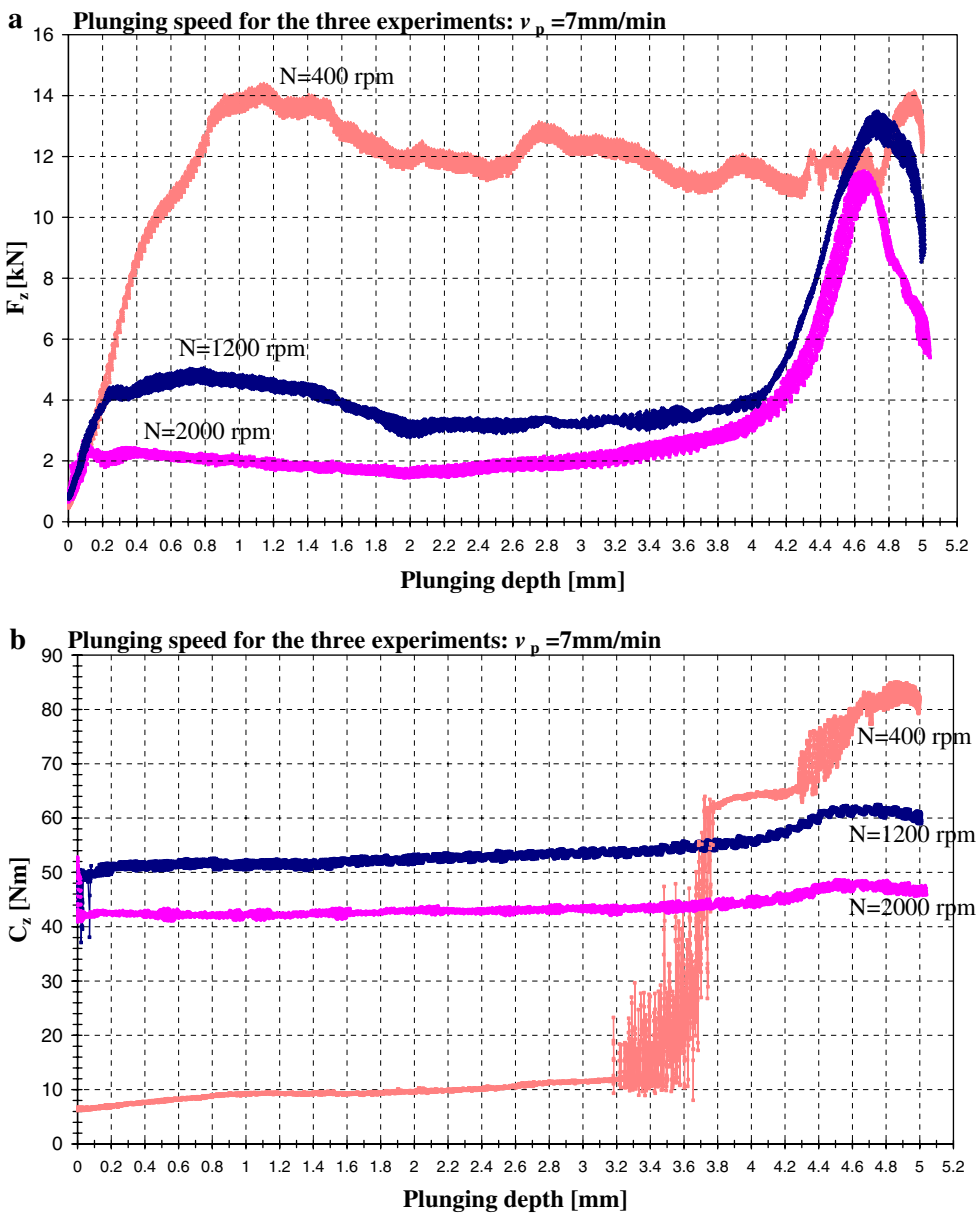

Fig. 14 **a** Axial force curves evolution for different processing parameters, **b** spindle torque curves evolution for different processing parameters

material mechanical interactions. Indeed, the torque curve evolution is different compared to the two others. For more than the half of the plunge depth, the torque is really low, under 10 Nm (Fig. 14b). It looks like no rotational resistance is applied on the tool, as if the tool is rotating without stirring the material around it. Then, the torque showed an abrupt change of evolution and increased sharply. It involves a sudden change of the tool/workpiece material mechanical interactions. The torque increase causes the modification of material flow around the tool due to sufficient heat input changing the material viscous characteristics. It can be assumed that the material stirring around the pin starts at this moment. The stirring generates material plastic deformation around the pin, increasing the rotational resistance and, consequently, the spindle torque. The curve shows that, when N_p=400 rpm, two different thermo-mechanical conditions had taken place around the tool, during the plunge stage. The same torque evolution is observed for the same rotational speed and different plunge velocity. Moreover, the same torque evolution was recorded for each tests performed, at identical processing parameters. As regarding the dissipated energy, $E_{dissipated}$, a significant energy input, i.e. heat input difference, can be noted depending on the rotational frequency. Table 1 presents the dissipated energy, calculated with Eq. 2, for the processing parameters v_p=7 mm/min, N_p=400, 1,200 and 2,000 rpm.

Table 2 presents the dissipated energy, as the tool has performed 1 mm of the plunging depth Δ_z. Between N_p= 400 rpm and N_p=1,200 or 2,000 rpm, a non-negligible

Table 1 Comparison between the dissipated energy for v_p=7 mm/min and N=2,000, 1,200 and 400 rpm and the maximum axial force and torque generated

N_p (tr/min)	$C_{z\ max}$ (Nm)	$F_{z\ max}$ (kN)	$E_{dissipated}$ (kJ)
400	85	15.5	36
1200	62	13.5	201
2000	49	11.5	329

v_p=7 mm/min

energy difference is recorded. It can be assumed that, at the plunge beginning, for N_p=400 rpm, the frictional heat input is not sufficient in order to start the material stirring. It leads to different thermo-mechanical tool/workpiece conditions, i.e. different temperature and different tool/workpiece mechanical interactions. Hence, the material does not soften enough, which causes higher axial force intensities and torque unusual behaviour.

7.3 Position of axial force and torque maximum

As $F_{z\ max}$ and $C_{z\ max}$ are characteristic for a static qualification of a FSW machine, it is important to investigate in depth the localisation of their peak according to the plunging depth. Based on 60 plunging tests, the analysed data showed that the maximum torque and axial force occurred when 94.5% and 97% of the plunge depth was accomplished, respectively. So, they both occur at the end of the plunge. At a total plunging depth of 5 mm, this peak localisation difference is 0.13 mm, negligible compared with measured response and error. Therefore, it can be concluded that for a static qualification of a FSW machine, the maximum axial force and torque should be considered simultaneously.

7.4 Influence of N_p and v_p on the output parameters

7.4.1 Analysis of the $F_{z\ max}$ and $C_{z\ max}$ according to N_p and v_p

Figure 15 presents the evolution of $F_{z\ max}$, $C_{z\ max}$ and the dissipated energy according to N_p for v_p set up at different values, 7, 14, 20, 27 and 35 mm/min, respectively. The experimental results demonstrate that the maximum axial force and torque can be influenced by both N_p and v_p. Two general tendencies can be identified. The first one is for a given N_p, the values of $F_{z\ max}$ and $C_{z\ max}$ increases as v_p increases. The second tendency is for a given v_p, as N_p increases, the maximum forces and torques decrease.

In Fig. 15a, b, it can be observed that the lowest axial force is associated with the lowest torque, and the highest axial force is associated with the highest torque. This is due to the generated thermo-mechanical interactions between the tool and the workpiece.

The analysis of the three diagrams of Fig. 15 presents two ways to reduce $F_{z\ max}$ and $C_{z\ max}$:

- At constant rotational speed by reducing the plunging speed v_p (Fig. 15a, b). It leads to an increase of the dissipated energy (Fig. 15c). Therefore, it increases the tool and workpiece temperature in the plunge zone. This leads to material softening facilitating the tool immersion and lowering the rotational resistance. In consequence, lowest maximum torque and axial force are recorded.
- At constant plunging speed v_p, an increase of the rotational speed leads to a decrease of the maximum spindle torque and axial force (Fig. 15a, b). Highest rotational speed involves a heat input increase by friction and therefore a greatest dissipated energy (Fig. 15c). So, an increase of the rotational speed involves a decrease of the rotational drag. This torque tendency, according to the rotational speed, has also been observed in the welding stage by Arora et al. [13].

So, a relation between the dissipated heat energy and the values of $F_{z\ max}$ and $C_{z\ max}$ can be visualised. And, the dissipated heat energy, and therefore the workpieces' material temperature and state, depends on the processing parameters. Moreover, the dissipated energy during this stage will influence the beginning of the welding stage [6, 12, 14]. Zhang and Zhang [14] studied the influence of the pre-heating time and the related temperature and strain rate on successful welding beginning. They showed that insufficient temperature rise and insufficient plastic deformation lead to defect formation in the welding beginning. But excessive preheating time leads to the tool penetration inside the workpiece in welding beginning stage [14]. In FSW, the global workpieces' pre-heating can be decomposed into two stages, the plunging stage and the dwell time. After these two stages, the tool begins to move along the joint line [4]. Therefore, to avoid defects and to guarantee successful welding, it is important to adapt the plunge and dwell time processing parameters, according to required heat for the welding beginning. For example, by modifying the plunge rotational speed, it modifies the heat input without influencing significantly $F_{z\ max}$ (Fig. 15a, c). The objective is to start the welding process in the optimal thermo-mechanical conditions.

Table 2 Comparison of the dissipated energy for v_p=7 mm/min and N_p=2,000, 1,200 and 400 rpm, as the tool has performed 1 mm plunging depth

Δ_z=1mm	N_p=2,000rpm, v_p=7mm/min	N_p=1,200rpm, v_p=7mm/min	N_p=400rpm, v_p=7mm/min
$E_{dissipated}$ (kJ)	100	70	3.5
Axial force range (kN)	F_z≤2.6	F_z≤5	F_z≤14.5

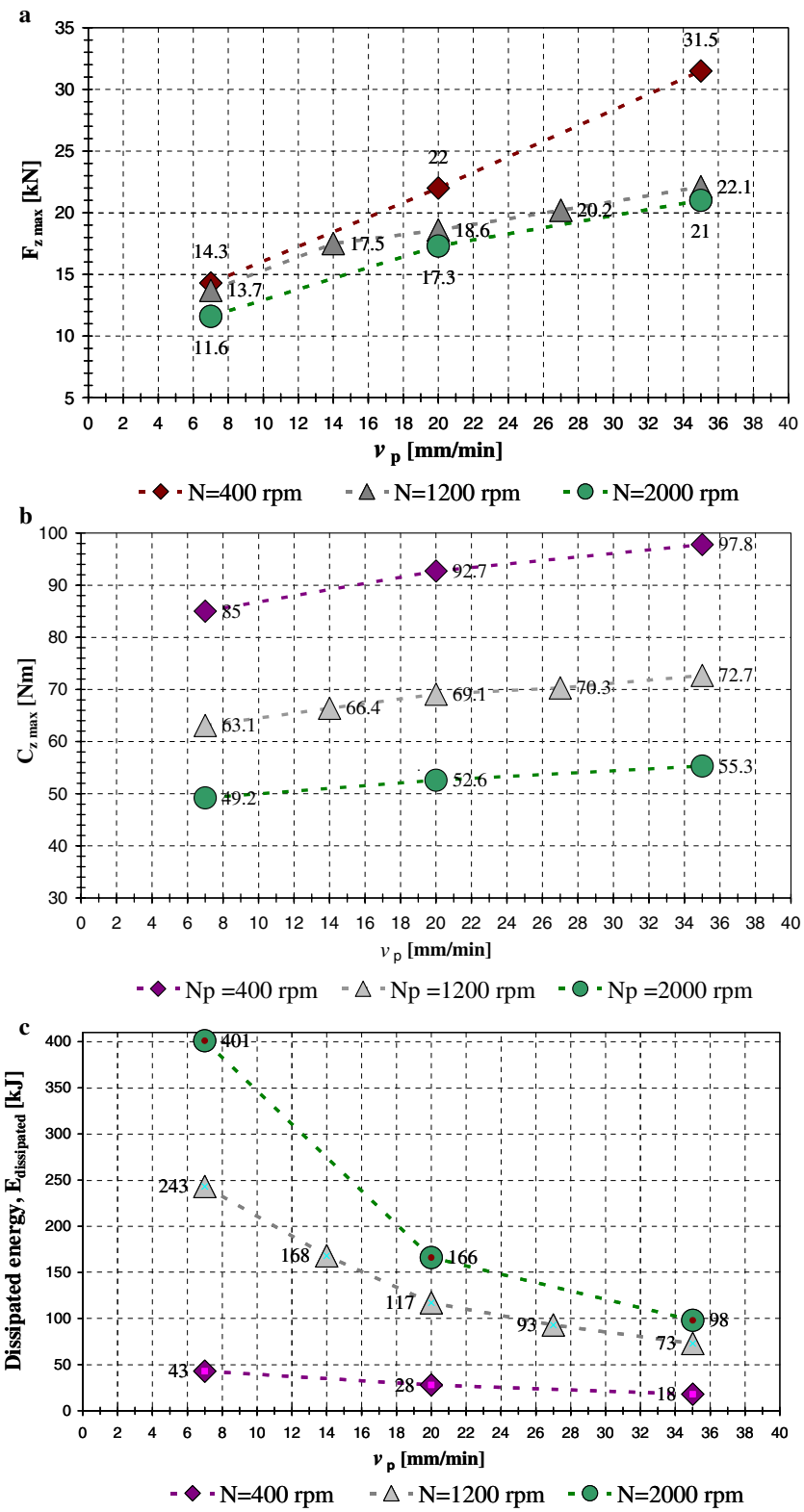

Fig. 15 **a** $F_{z\,max}$ evolution according to N_p for v_p set up as constant. **b** $C_{z\,max}$ evolution according to N_p for v_p set up as constant. **c** Dissipated energy during the plunging stage according to N_p for v_p set up as constant

All these observations lead to the conclusion that the heat input and the axial force and torque responses, occurring during the plunging stage, are a consequence of the tool/workpiece material mechanical interactions. These results are verified by the curves analysis (Figs. 16a, b and 14a, b). Thus, for identical processing parameters, the tool/workpiece thermo-mechanical interactions should be the same over the plunging depth, leading to identical forces

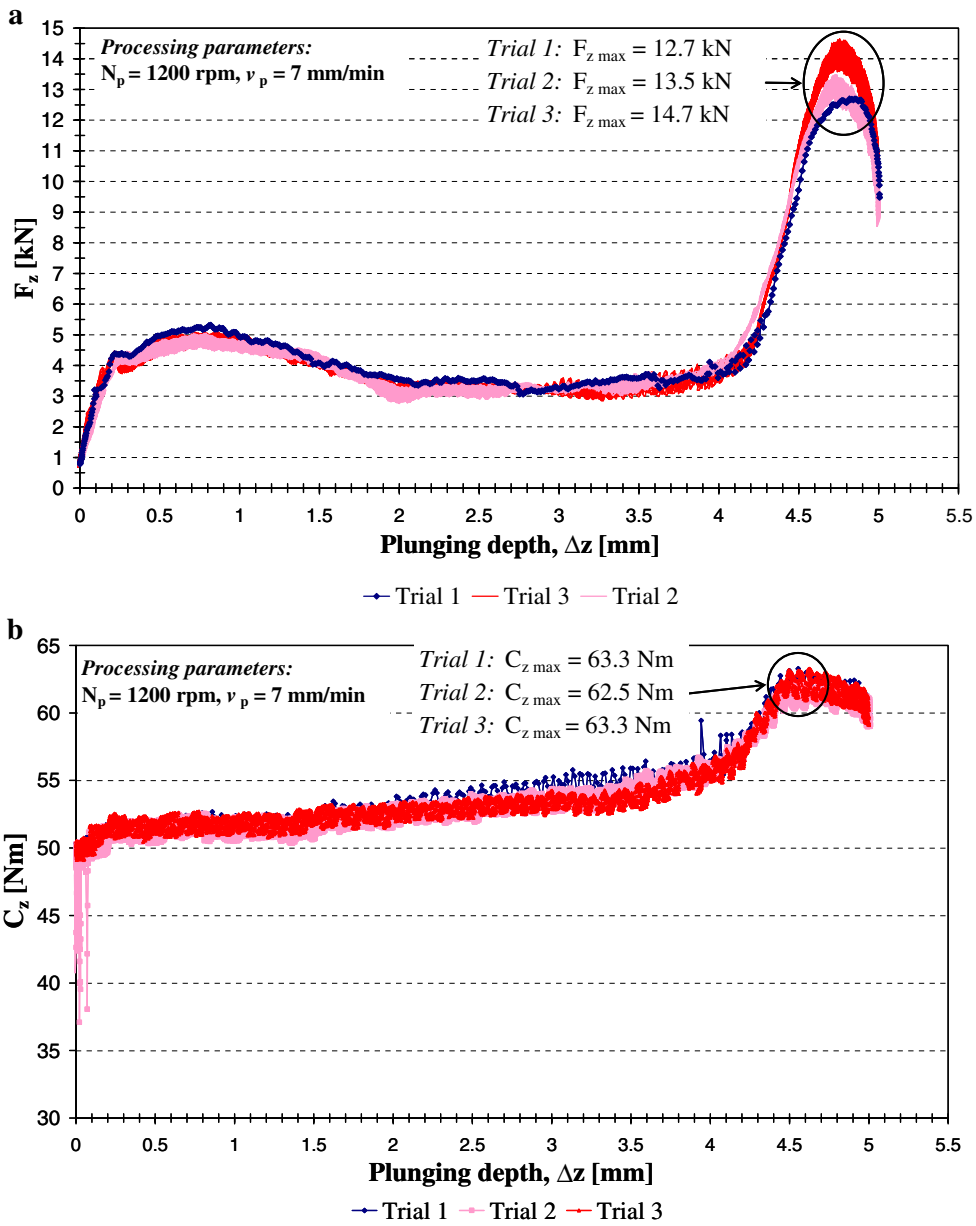

Fig. 16 Axial force evolution (**a**) and spindle torque evolution (**b**) for three trials done at same processing parameters

and torque evolutions and values. Figure 16a, b presents the forces and torque curves for three tests performed at same processing parameters. The force and torque peak location and the curves evolutions can almost be superimposed. It demonstrates that the tool/workpiece material mechanical interactions are identical and repeatable. It is an interesting observation for the qualification of a machine and the industrialisation of the welding process.

For three tests, performed at identical processing parameters, the maximum torque value is the same (Fig. 16b). This repeatability is observed for all sets of parameters, implying that the thermo-mechanical conditions around the tool are the same. However, differences on the measured $F_{z\ max}$ values could be observed (Fig. 16a).

As $F_{z\ max}$ is characteristic for the static qualification of FSW machine, it seems interesting to analyse its repeatability. Therefore, a study was preformed on 19 tests performed with the same processing parameters, the same tool and workpiece material. The $F_{z\ max}$ standard deviation from the mean value is about 0.8, which is negligible. But, the maximum peak amplitude difference registered was about 20%. This amplitude is not negligible and cannot only be explained by errors measurement. This variation should be taken into account for a FSW machine static qualification. To explain this maximum force variation, some hypothesis can be made. In theory, v_p and d_p are identical. So, the tool axial velocity should be the same from one test to another, as the shoulder touches the workpieces' top surface. But some differences in the tool

velocity, when the shoulder enters fully in contact with workpiece surface, could be different due to "real" speed control system. Small velocity differences could explain some force variation. Another factor could be added. As mentioned before, when the pin enters inside workpieces, some extruded material is displaced upward around the pin. The material volume and its repartition around the pin are certainly not the same from one test to another, leading to force variability when this material is squeezed under the tool shoulder (step 3, Fig. 13d–f). The combination of these two factors could explain a 20% axial force difference, from one test to another. Therefore, to qualify, from a static point of view, a FSW machine, a safety factor should be taken on the plunge maximum force value.

7.4.2 Analysis of the F_x and F_y according to N_p and v_p

F_x and F_y are the two other force components transmitted to the welding equipment. They are respectively in the (O,X) and (O,Y) directions defined in Fig. 2. As presented in Fig. 17, the curve analysis showed that F_x and F_y are oscillating around a mean value equal to zero. The oscillation maximum amplitudes are generally representing 10% to 20% of $F_{z\ max}$. The analysis also showed that the maximum values of F_x and F_y cannot be correlated to the processing parameters. The knowledge of the minimum and maximum values of F_x and F_y can be integrated to the static characterisation of a FSW machine. Moreover, it can be needed for the determination of the required clamping device.

As the plunge stage reaches step 3 (Figs. 12 and 13), i.e. when the shoulder enters in contact with the extruded material, the forces F_x and F_y encounter some oscillations. These oscillations are probably due to transversal load variation on tool caused by the non-homogeneous contact between the extruded material and the tilted shoulder. These forces variations generate some tool oscillations during the plunge experiments, certainly because the pin is not entirely inside the workpiece.

A frequency analysis has then been performed through a fast Fourier transform analysis. Into the F_x and F_y oscillations, there are some low frequencies, probably related to the FSW machine hydraulic system, and one frequency corresponding to the tool rotational speed. Figure 18 presents the numerical results.

It seems important to take into account the force oscillating phenomena because these could impact the FSW machine and clamping devices on a vibration point of view. The vibrations will principally impact the machine on the beginning of the plunge when the pin is not fully immersed into the workpiece.

7.5 Experimental plunging test diagram

By analysing the maximum axial forces over the experimental range, it appears that "force ranges" could be identified. The diagram presented in Fig. 19 can be used to select the appropriate sets of parameters, depending on the forces and torque capacities of the available machine. It can also be used to select the best compromise between the developed force and torque and the stage productivity. In Fig. 19, arbitrary force ranges are presented.

These kinds of results are interesting to choose the appropriate sets of parameters to perform friction stir spot welding. For a given FSW configuration, this diagram

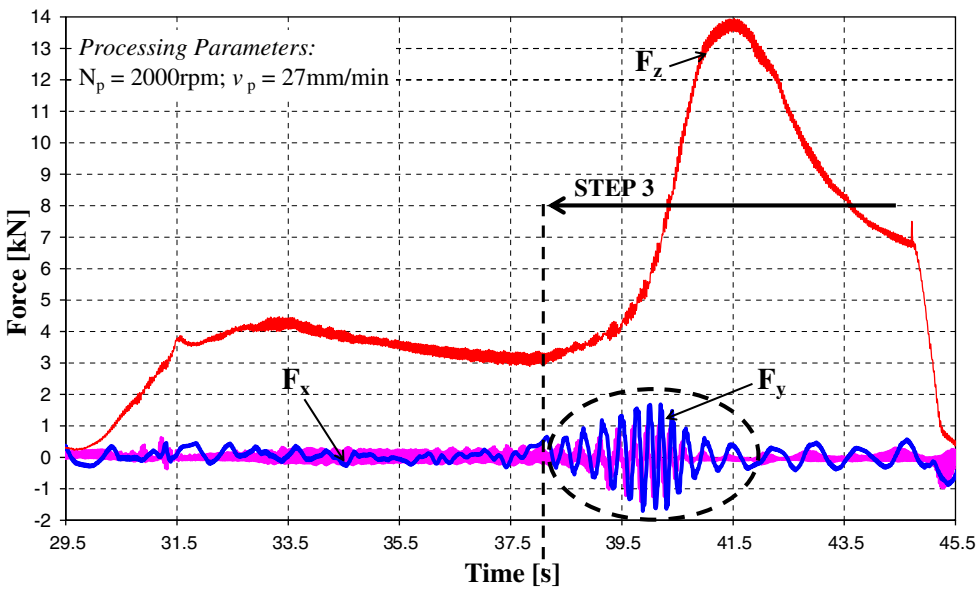

Fig. 17 Evolution of the forces F_z, F_x and F_y according to the time

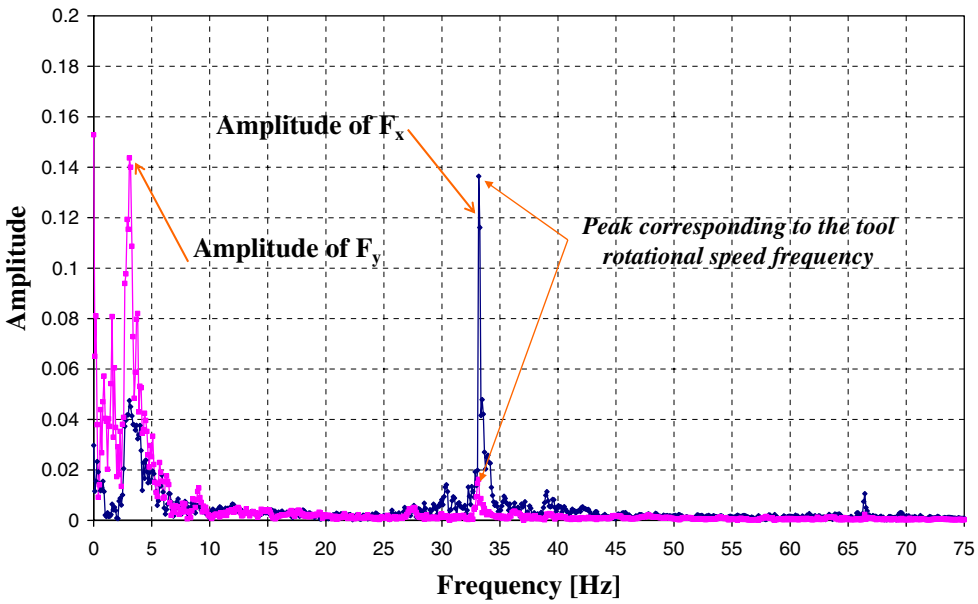

Fig. 18 Results of the fast Fourier transform of the forces F_x and F_y

combined with the process window will entirely define the welding process. These diagrams may play a key role for industrial scale use of FSW.

This work also suggests that the tool rotational frequency used to perform the plunging and the welding stages could be parameterised at different values. The final goal is to combine the plunge objectives, e. g. to obtain low axial force, with the realisation of a high weld quality. It will probably imply different rotational frequencies, according to the stage.

8 Conclusion

The maximum axial force and torque occurring during the plunging stage are characteristic for a FSW machine qualification. Therefore, experimental plunging tests were performed. The analysis showed that the maximum axial force and torque can be influenced by both N_p and v_p. These results show a way to reduce their maximum amplitude without drilling a hole before starting the plunging stage. It illustrates a way to find processing parameters enabling or widening

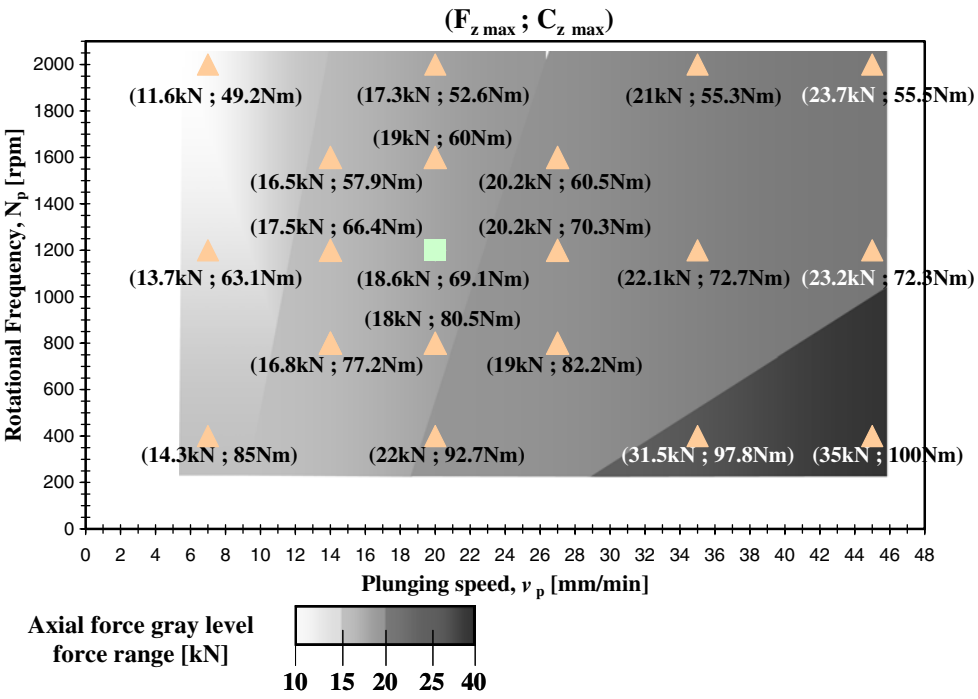

Fig. 19 Maximum axial force and spindle torque according to N_p and v_p

the use of standard and flexible welding equipment, allowing the FSW of complex geometries.

The curves evolution analysis showed that the axial force and torque evolution throughout the plunging stage are a consequence of the applied processing parameters. In fact, the processing parameters affect the generated heat by friction and plastic deformation leading to different tool/workpiece mechanical interactions. So, a relation between the dissipated heat, the axial force and torque response was observed. As, the dissipated heat energy was too small, the material applied more resistance on the tool, generating greater forces and torque.

The analysis also demonstrate that the tool/workpiece thermo-mechanical interactions are repeatable from one test to another, leading to similar forces and torque curve evolutions throughout the stage. The torque amplitude repeatability from one test to another at same processing parameters was observed. But, the maximum axial force amplitude showed some variation, from one test to another at same processing parameters. It implies to take a force safety factor for the static qualification of the FSW machine.

To facilitate the plunge processing parameter choice, a diagram presenting the maximum axial force and torque according to the processing parameters can be used. It allows the selection of the plunge processing parameters according to the required productivity and the available machine capacities.

The presented experimental results depend on the used tool geometry, the work material and thickness. However, the obtained results are general material behaviour, and the analysis realised for the 6082-T651 could be related to comparable aluminium alloys of the 6xxx series. Moreover, the described influence of $F_{z\ max}$ and $C_{z\ max}$, according to the processing parameters, are probably the results of the combination of the generated heat by the tool/workpiece mechanical interactions. Therefore, they could be generalised. So, the effects observed could be applied to other, heat-treatable aluminium alloys. But, their values depend on the tool geometry and especially on the shoulder diameter.

9 Future work

Future work will be to perform the analysis on other heat treatable and non-heat-treatable aluminium series. The objective is to watch if the results presented in this paper could be generalised to other aluminium alloys.

The future work will also be focussed on the investigation of the thermo-mechanical phenomenon, leading to the uncharacteristic force and torque behaviour highlighted in this paper.

The main stages during friction stir welding are the plunge, the dwell and the welding. To perform a defect-free and good quality weld, it is essential to harmonise the processing parameters of these three stages. Therefore, the future work is to analyse the influence of the processing parameters on the transition, plunging and welding stages. The objective is to find plunging and welding processing parameters, permitting the use of standard and flexible welding equipment. This equipment should allow the FSW of complex geometries and the specified weld quality. The combined use of a plunging diagram and the process windows will make it possible. So, the whole welding process will be considered.

Acknowledgements The authors would like to thank the Region Lorraine and the Moselle department for their financial support for this research project. They also want to thank Daniel Strina for his technical support and Patrick Martin for his fruitful scientific discussions.

References

1. Thomas WM, Nicholas ED., Needham JC, Murch MG, Templemith P, Dawes CJ (1991) Patent Application No. 9125978.8
2. Mishra RS, Ma ZY (2005) Friction stir welding and processing. Mater Sci Eng R 50:1–78
3. Arbegast WJ (2007) Friction stir welding and processing (Chapter 13). ASM International, Materials Park, OH, ISBN-13978-0-87170-840-3
4. Zimmer S, Langlois L, Laye J, Goussain JC, Martin P, Bigot R (2008) Methodology for qualifying a friction stir welding equipment. Proceedings of the 7th International Symposium on Friction Stir Welding, Awaji Island, Japan
5. Lienert TJ, Stellwag WL,. Grimmett BB, Warke RW (2003) friction stir welding studies on mild steel. Supplement to the Welding Journal, January 2003
6. Mandal S, Rice J, Elmustafa AA A (2008) Experimental and numerical investigation of the plunge stage in friction stir welding. J Mat Process Technol 203:411–419
7. Fourment L, Guerdoux S (2008) 3D numerical simulation of the three stages of friction stir welding based on friction parameters calibration. Int J Mater Form Suppl 1:1287–1290
8. Zhang Z, Zhang ZW (2007) Numerical studies on effect of axial pressure in friction stir welding. Sci Technol Weld Join 12(3):226–24
9. Santella M, Grant G, Arbegast W (2003) Plunge testing to evaluate tool materials for friction stir welding of 6061+20wt% Al2O3 composite. Proceedings of the 4th International Symposium on Friction Stir Welding, Part City, USA
10. Gerlich A, Su P, North TH (2005) Tool penetration during friction stir spot welding of Al and Mg alloys. J Mater Sci 40:6473–6481
11. Zaeh MF, Eireiner D, Papadakis L (2005) Friction stir welding with modern milling machines. Requirements, Approach and Application. Proceedings of the 5th International Symposium on Friction Stir Welding, Metz, France
12. Soundararajan V, Zekovic S, Kovacevic R (2005) Thermo-mechanical model with adaptive boundary conditions for friction stir welding of Al 6061. Int J Mach Tools Manuf 45:1577–1587
13. Arora A, Nandan R, Reynolds AP, Debroy T (2009) Torque, power requirement and stir zone geometry in friction stir welding through modeling and experiments. Scr Mater 60:13–16
14. Zhang Z, Zhang ZW (2007) Numerical studies of preheating time effect on temperature and material behaviours in friction stir welding process. Sci Technol Weld Join 12(5):436–448